

The Effect of Rare-Earth Metal Oxide Additives on Crack Growth Resistance of Fine-Grained Partially Stabilized Zirconia



V. V. Kulyk, Z. A. Duriagina, B. D. Vasylyv, V. I. Vavrukh, T. M. Kovbasiuk, P. Ya. Lyuty, and V. V. Vira

Abstract Recently, the additives of rare-earth metal oxides are being used for obtaining partially stabilized zirconia ceramics aimed at applications in various high-temperature structural components. Corresponding sintering modes providing fine-grained microstructure formation are being developed. Due to the obtained correlations between the morphology parameters and resulting mechanical characteristics of ceramics, it is possible to reach a unique combination of their functional properties. In this work, zirconia ceramics stabilized with small percentages of rare-earth metal oxides have been studied in terms of sintering ability, elimination of the phase changes in zirconia, as well as employment of the transformation toughening mechanism during crack propagation. The metal oxides including rare-earth metal oxides (Y_2O_3 , CoO , CeO_2 , Fe_2O_3) were used as additives to reach a stabilizing effect on zirconia and manufacture ceramics with fine-grained microstructure. Series of ceramic specimens were prepared using conventional sintering in a temperature range of 1550–1620 °C. Fracture toughness test by indentation method and single-edge notch beam test under three-point bending were performed. Based on X-ray diffraction analysis and SEM studies of fracture surfaces of specimens, it was

V. V. Kulyk (✉) · Z. A. Duriagina · V. I. Vavrukh · T. M. Kovbasiuk · P. Ya. Lyuty
Department of Materials Science and Engineering, Lviv Polytechnic National University, 12 S. Bandera Str., Lviv 79013, Ukraine
e-mail: kulykvolodymyrvolodymyrovych@gmail.com

Z. A. Duriagina
Department of Materials Engineering, The John Paul II Catholic University of Lublin, 14 Raławickie Al., 20-950 Lublin, Poland

B. D. Vasylyv
Department of Hydrogen Technologies and Alternative Energy Materials, Karpenko Physico-Mechanical Institute of the NAS of Ukraine, 5 Naukova Str., Lviv 79060, Ukraine

V. V. Vira
Department of Strength of Materials and Structural Mechanics, Lviv Polytechnic National University, 12 S. Bandera Str., Lviv 79013, Ukraine

concluded that the maximum transformation toughening effect revealed for $\text{ZrO}_2\text{--Y}_2\text{O}_3\text{--CoO--CeO}_2\text{--Fe}_2\text{O}_3$ ceramics was related to a distinct change in the fracture surface pattern.

1 Introduction

Nowadays, zirconia ceramics doped with the stabilizing oxides Y_2O_3 [1–4], CeO_2 [5–7], MgO [8], or CaO [9] are being widely developed. The metastable tetragonal phase of zirconia ceramics is stabilized in such a way at room temperature. It is well known that transformation toughening of zirconia occurs due to the transformation of the tetragonal (t) phase into the monoclinic (m) one [10–14]. This process takes place in the crack tip vicinity under significant stresses, which can effectively improve crack growth resistance of ceramics. Therefore, increased strength and crack growth resistance of the ceramics can be ensured due to the tetragonal phase.

Additionally, other oxides can be added while producing these ceramics to improve their mechanical strength and physical properties [10, 15–25]. Partially stabilized zirconia ceramics having improved mechanical properties can be utilized in various high-temperature structural components [26–30]. These ceramics are also widely used in energy generation, chemical industry, and biomedical applications [31–42].

The authors of a number of works [43–45] showed that the sintering temperature may affect to a great extent the grain size, porosity, and mechanical behavior of zirconia. It was reported in the work [44] that a single-phase microstructure (m- ZrO_2) had been formed already after pressing the zirconia specimens without Y_2O_3 additive. In contrast, ceramics containing 1.5 mol% Y_2O_3 exhibited a single-phase microstructure (t- ZrO_2) after sintering at 1100 °C. As compared to the two last variants, for zirconia containing 8 mol% Y_2O_3 , a single-phase microstructure (c- ZrO_2) was formed during pressing. The maximum pore diameter in all the compacts reached 12.5 nm after pressing. An increase in the pore diameter was found in specimens without Y_2O_3 additive when the temperature increased to 600 °C. Intense grain growth and lowering of porosity occurred with a further increase in sintering temperature to 1100 °C. In a similar way, specimens containing 1.5 and 8 mol% of Y_2O_3 additives exhibited significant pore growth with increasing the sintering temperature to 600 °C. Significant densification of the specimens, along with the slight growth of grains, was revealed with increasing temperature up to 1100 °C.

Several authors investigated the effect of conditions of zirconia ceramics preparation on the resulting grain size and mechanical behavior of prepared specimens [46–50]. The authors of the work [47] studied the evolution of grain growth in doped zirconia annealed at 1500 °C for several hours. The maximum grain size for 12Ti- ZrO_2 ceramic was found to reach while sintering at 1400 °C with for 70 h. Other authors [48] reported grain size of about 1 μm while sintering at 1500 °C for a few hours. In the work [49], a study on the grain growth of zirconia ceramics was performed. A maximum grain size of 20 μm was found for 8 mol% $\text{Y}_2\text{O}_3\text{--ZrO}_2$

ceramic after sintering at 1700 °C for 20 h. For Y_2O_3 - ZrO_2 ceramic containing 4 mol% Y_2O_3 , a maximum grain size of more than 11 μm was found after sintering at 1800 °C for 100 h. The authors of the work [50] investigated specimens of zirconia ceramics sintered at maximum temperature 1600 °C for 2 h. It was found that the maximum mean grain size is 0.35 μm .

Several scientists applied spark plasma sintering as one of the recently developed techniques for preparing bulk zirconia-based ceramics, namely ceria stabilized zirconia [51–53], yttria-stabilized zirconia [54, 55], and other ceramics [56–59].

In the work [60], the influence of the zirconia percentage on the crack growth resistance and strength of Al_2O_3 - ZrO_2 ceramics was studied. The ceramics consisted of the monoclinic and tetragonal ZrO_2 phases and the α - Al_2O_3 phase. The percentage of the t- ZrO_2 phase decreased with increasing the total amount of ZrO_2 . The formation of fine-grained Al_2O_3 - ZrO_2 microstructure was reached due to adding 10–20% ZrO_2 that allows obtaining ceramics with improved mechanical properties. It was proven in the work [61] that mechanical properties of alumina doped with zirconia and yttria-stabilized zirconia can be effectively optimized due to both the flexural strength and fracture toughness determination.

The authors of the works [62, 63] studied YSZ ceramics stabilized with 3–5 mol% Y_2O_3 . The chemical and phase compositions of the ceramics were found to relate to their mechanical properties [64]. 5YSZ ceramics sintered at 1450 °C for 2 h exhibited the highest fracture toughness. This is consistent with a comparatively high percentage of the tetragonal ZrO_2 phase [62]. Effects of the sintering mode and phase composition on mechanical behavior of YSZ ceramics doped with 6–8 mol% Y_2O_3 were studied in the work [63]. After sintering at 1600 °C for 2 h, 7YSZ ceramics showed the highest fracture toughness, similarly to the results published in [65].

In the work [66], correlations between the yttria percentage, phase balance, grain size distribution, morphology of the fracture surface, and strength for zirconia with addition of 3 to 8 mol% Y_2O_3 (YSZ ceramics) sintered at 1550 °C for 2 h in argon were analyzed. It was shown that 7YSZ ceramic containing the monoclinic and tetragonal ZrO_2 phases exhibited the fine-grained microstructure and, as a result, the highest strength.

This work is aimed at studying the effects of oxide additives and sintering temperature on the microstructure, microhardness, strength, and fracture toughness of fine-grained ZrO_2 - Y_2O_3 - CoO - CeO_2 - Fe_2O_3 ceramics for various applications.

2 Materials and Methods

In this work, zirconia ceramics stabilized with oxides Y_2O_3 , CoO , CeO_2 , and Fe_2O_3 have been studied.

Three series of beam specimens of partially stabilized zirconia (PSZ) approximately $2.9 \times 2.9 \times 45 \text{ mm}^3$ in size were sintered in an argon atmosphere for 2 h at temperatures of 1550 °C, 1580 °C, and 1620 °C, respectively. An electric resistance furnace was used for sintering. For marking each series, corresponding sintering

temperatures were indicated, i.e., PSZ–1550, PSZ–1580, and PSZ–1620 (Table 1). To avoid phase transformations, the side surfaces of specimens after sintering were processed using a grinding and polishing machine for metallographic preparation. Such processing allowed reaching the required surface quality.

To measure microhardness of the studied ceramics, a NOVOTEST TC-MKB1 microhardness tester was used. At least ten indentations under each of the indentation load of 0.25 N, 0.49 N, 0.98 N, 1.96 N, 2.94 N, 4.91 N, and 9.81 N were made to determine the microhardness of the ceramics under study. The test was performed according to the relevant standards [67–69].

Various teams of scientists around the world have developed a large number of formulas for calculating the microhardness of brittle materials [70–79].

Vickers microhardness (in GPa) was calculated using the formula [68]:

$$H = 0.0018544 \left(\frac{P}{d^2} \right), \quad (1)$$

where P is the indentation load (N) and d is the average length of the diagonals of the indentation imprint (mm).

The geometries of imprint and crack were estimated using an optical microscope Neophot-21.

To estimate fracture toughness of the ceramics, the critical stress intensity factor (SIF), K_{Ic} , was calculated as an indicator of the propensity of ceramics to brittle fracture [62, 80]. It is known about a number of methods for evaluating the fracture toughness of ceramics and cermets using Vickers indentation [81–83]. The developed formulas used for the K_{Ic} value calculation include both mechanical and physical characteristics, as well as experimentally determined coefficients. Recently, it was proven in the works [63, 84] that for the characterization of the ZrO_2 – Y_2O_3 ceramics, the formula developed in [81] provides the best convergence of results with those obtained by traditional methods of fracture mechanics. This formula used in our work is as follows:

$$K_{Ic} = 0.016 \left(\frac{E}{H} \right)^{1/2} \left(\frac{P}{c^{3/2}} \right), \quad (2)$$

where E is Young's modulus (GPa), H is microhardness (GPa), P is the indentation load (N), and c is the radial crack length (m).

Table 1 Marking of the investigated ceramics, their chemical compositions, and sintering modes

Series marking	System and chemical composition, mol%	Sintering mode	
		temperature, °C	Time, h
PSZ–1550	90ZrO ₂ –1Y ₂ O ₃ –1CoO–7CeO ₂ –1Fe ₂ O ₃	1550	2
PSZ–1580	90ZrO ₂ –1Y ₂ O ₃ –1CoO–7CeO ₂ –1Fe ₂ O ₃	1580	2
PSZ–1620	90ZrO ₂ –1Y ₂ O ₃ –1CoO–7CeO ₂ –1Fe ₂ O ₃	1620	2

To study mechanical behavior of the ceramics, the three-point flexure test of ceramic specimens was performed in air at 20 °C with calculating fracture stresses [85, 86].

For comparison with the Vickers indentation method, a single-edge notch beam (SENB) test [87–89] was carried out as a conventional method of estimating the fracture toughness of the ceramics. The notch width was 0.1 mm. The SENB specimens were tested under three-point bend at 20 °C in air [90–99]. Corresponding formulas given elsewhere [87–89] were used for calculating the critical SIF K_{Ic} of the ceramics.

In both the cases (SENB and Vickers indentation tests), the average K_{Ic} value of five specimens for each series was calculated.

The microstructure and fracture surface analyses of material specimens were carried out using a Carl Zeiss EVO-40XVP scanning electron microscope (SEM). For an energy-dispersive X-ray (EDX) microanalysis, an INCA Energy 350 system was used. X-ray diffraction (XRD) analysis of specimens was performed on a DRON-4.07M diffractometer. The WinCSD program package was used to perform the procedures of indexing, refinement, and calculation of the zirconia phase weight percentages.

3 Results and Discussion

The phase compositions of the studied ceramics were determined based on the XRD analysis.

The XRD patterns for the studied ceramics exhibited two-phase structure with clear peaks of the t-ZrO₂ and m-ZrO₂ phases (Fig. 1). It was found that the peak heights of the t-ZrO₂ phase slightly increased for the material sintered at a temperature of 1580 °C, compared to that sintered at 1550 °C, whereas the peak heights of the m-ZrO₂ phase slightly decreased. Even more increase of peaks of the t-ZrO₂ phase and lowering of peaks of the m-ZrO₂ phase were observed for the material sintered at 1620 °C.

Such differences in the peak heights for obtained XRD patterns are consistent with the phase balance in the studied ceramics (Fig. 2). For ceramics sintered at 1550 °C, tetragonal phase fraction was about 82.6%, whereas for ceramics sintered at 1580 °C and 1620 °C, the fractions were 84.6% and 85.9%, respectively. For these ceramic series, monoclinic phase fractions were about 17.4%, 15.4%, and 14.1%, respectively. Therefore, correlations between the sintering temperature for the studied materials and percentages of the t-ZrO₂ and m-ZrO₂ phases were observed.

There are lots of works on microstructure-related microhardness and strength of zirconia-based ceramics [84, 92, 99–106]. For ZrO₂–8 mol% Y₂O₃ ceramics [63, 84], a gradual decrease in microhardness with an increase in the indentation load from 0.49 to 9.81 N was found. Such material behavior evidences the indentation size effect peculiar to ceramics [107]. However, the microhardness values for ZrO₂–8 mol% Y₂O₃ ceramics were found to yield on the plateau at the loads in a range of

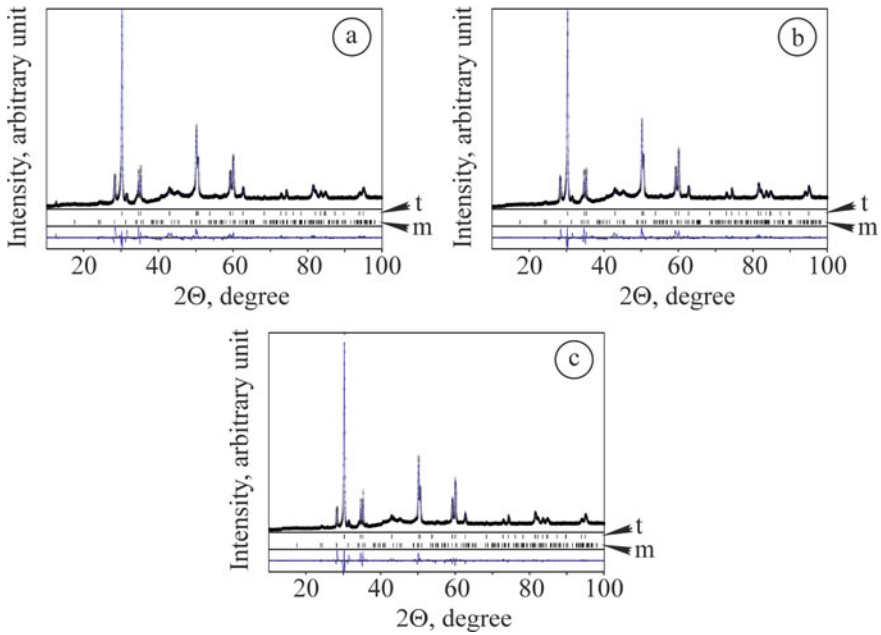
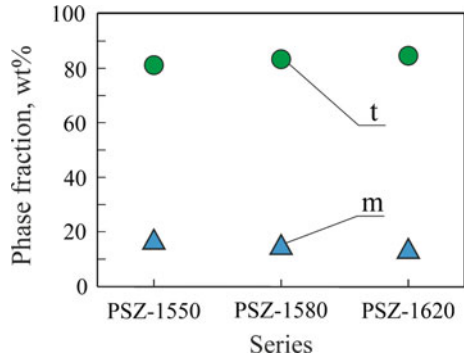


Fig. 1 XRD patterns of the studied ceramics (Table 1). Notation: t is tetragonal and m is monoclinic ZrO₂

Fig. 2 Phase balance in the studied ceramics (Table 1). Notation: t is tetragonal and m is monoclinic ZrO₂

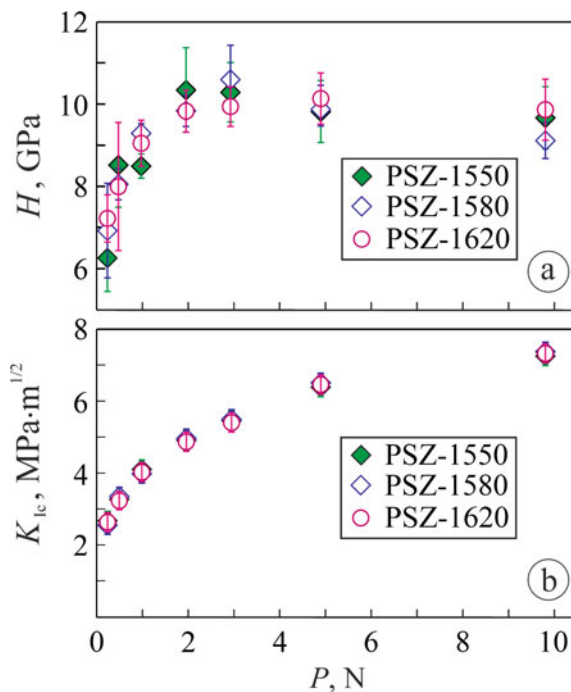


4.91–9.81 N. Such a phenomenon allows concluding that the values of microhardness and fracture toughness in this loading range are invariant.

In our work, the indentation loads of 0.25 N, 0.49 N, 0.98 N, 1.96 N, 2.94 N, 4.91 N, and 9.81 N were set and corresponding microhardness values were determined for the studied materials 1–3 (Fig. 3a).

The obtained microhardness vs load correlations are similar and can be divided into two parts. The first part of each dependence corresponds to low indentation loads (up to 0.98 N), whereas the second one corresponds to the range of 1.96–9.81 N.

Fig. 3 Changes in mechanical characteristics of the studied ceramics depending on the indentation load: **a** Vickers microhardness; **b** fracture toughness measured by the Vickers method. The symbol marking corresponds to the series marking given in Table 1

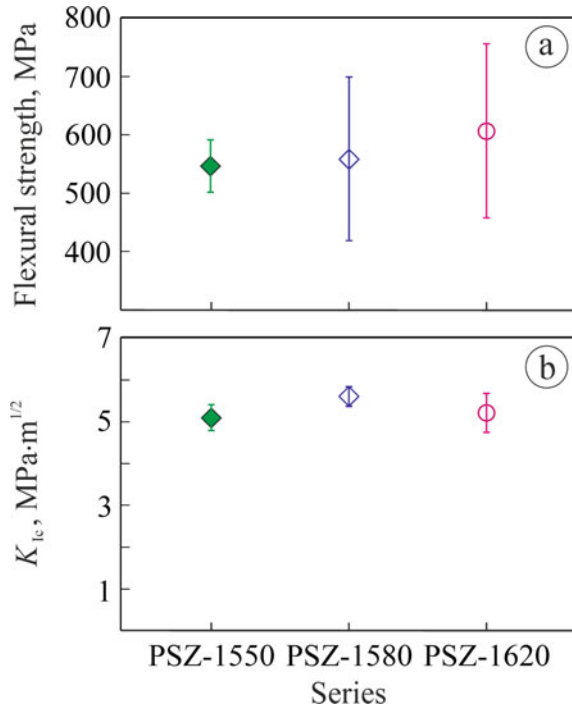


In this range, the above-mentioned indentation size effect is observed. In contrast, the first part of each dependence exhibits the lowered microhardness values due to the indentation imprints commensurable with the average diameter of pores on the specimen surface. The average microhardness values for all the studied materials were revealed to yield on the plateau under the loads of 4.91–9.81 N (Fig. 3a). For this load range, a trend to increase invariant values of microhardness with an increase in the sintering temperature was found.

It is known that an increase in sintering temperature leads to intensive grain growth in yttria-stabilized zirconia. When the average grain size of the t-ZrO₂ phase becomes larger than the admissible one (about 1 μm for ceramics of this type), the retention of the metastable tetragonal zirconia is suppressed [108]. As the microhardness of t-ZrO₂ is higher than m-ZrO₂ [108], the lowering of microhardness occurs during indentation, due to the t–m transition. In our case, the t-ZrO₂ phase is stabilized mainly with CeO₂, in which content in the ceramics is 7 mol%. Such a CeO₂ amount allows the strong stabilization of the tetragonal crystal structure to be achieved. A slight decrease in the m-ZrO₂ phase fraction with an increase in sintering temperature of the ceramics (Fig. 2) is consistent with a slight increase in the microhardness of the ceramics (Fig. 3a).

To construct a graph for studying the changes in fracture toughness of the ceramics with a change in the sintering temperature from 1550 °C through 1580 °C to 1620 °C, the values of the material microhardness obtained under the indentation load in the

Fig. 4 Changes in mechanical characteristics of the studied ceramics (Table 1): **a** flexural strength; **b** fracture toughness measured by the SENB method under three-point bending



range of 0.25–9.81 N were taken (Fig. 3b). Surprisingly, a slight difference between obtained levels of fracture toughness for the studied materials was found.

In contrast to such a little difference in values of fracture toughness measured by the Vickers method for the studied materials, distinct changes in both the flexural strength and fracture toughness measured by the SENB method under three-point bending while increasing the sintering temperature were found (Fig. 4).

It should be noted that the ceramic sintered at 1550 °C has both the lowest flexural strength and fracture toughness measured by the SENB method (Fig. 4). No significant difference in fracture toughness was found for all the studied ceramics. However, the best result was obtained for the ceramic sintered at 1580 °C (Fig. 4b). It is assumed that in such conditions, the highest bond strength between recrystallized t-ZrO₂ grains is achieved. Although no distinct difference was revealed at low magnifications in the microstructure images (Fig. 5a, c, e) and corresponding images of fracture surfaces (Fig. 5b, d, f), the above assumption is confirmed by the images of microstructure (Fig. 6a, c, e) and fracture surfaces (Fig. 6b, d, f) taken at high magnifications. In particular, slightly increased t-ZrO₂ grains are observed in the ceramic sintered at 1580 °C compared to those in the ceramic sintered at 1550 °C.

Besides, no signs of transgranular fracture of the m-ZrO₂ phase particles were found in the ceramic sintered at 1580 °C (Fig. 6d), whereas in that sintered at 1620 °C a comparatively large number of cleavage facets were revealed (Fig. 6f). This obviously is a reason for the lower fracture toughness of the last material series.

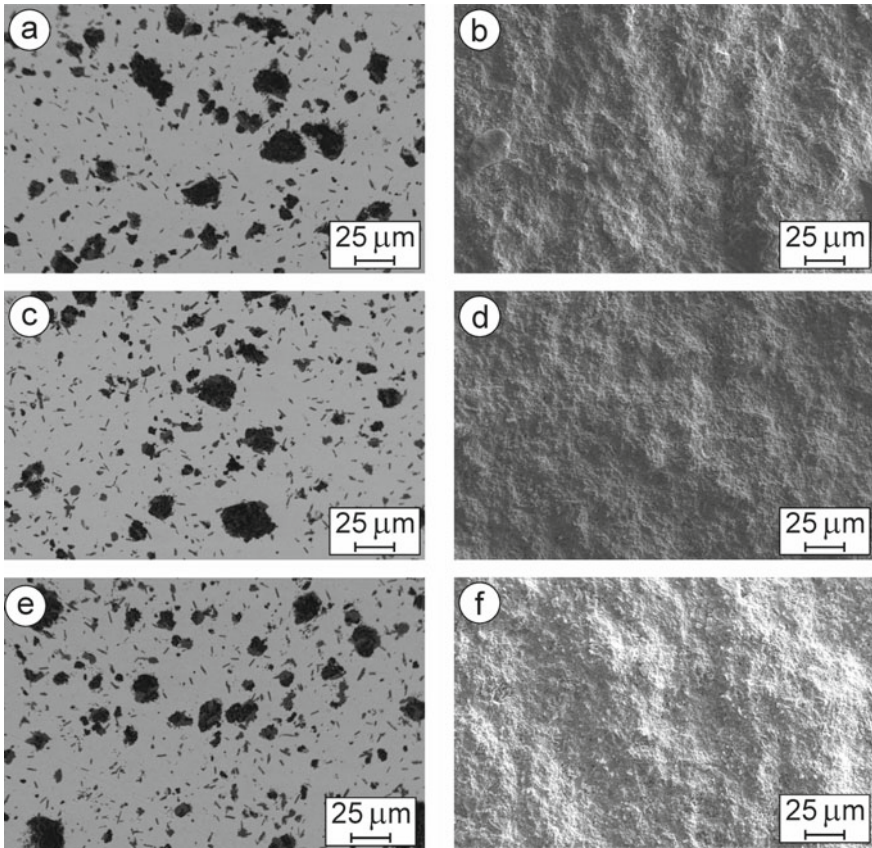


Fig. 5 SEM **a, c, e** microstructures (BSD images at low magnifications) and **b, d, f** fractography (SE images at low magnifications) of specimen series **a, b** PSZ-1550, **c, d** PSZ-1580, and **e, f** PSZ-1620 (Table 1)

The weaker areas consisting of freely transformed $m\text{-ZrO}_2$ grains adjoin the coarse particles of the $m\text{-ZrO}_2$ phase in the ceramic sintered at 1620 °C. Such local weakening affects the fracture toughness of the material by lowering it. In contrast, no effect of the local weakening on flexural strength of this ceramic was found. Therefore, coarse particles of the $m\text{-ZrO}_2$ phase contribute dominantly to increasing the strength of a bulk material.

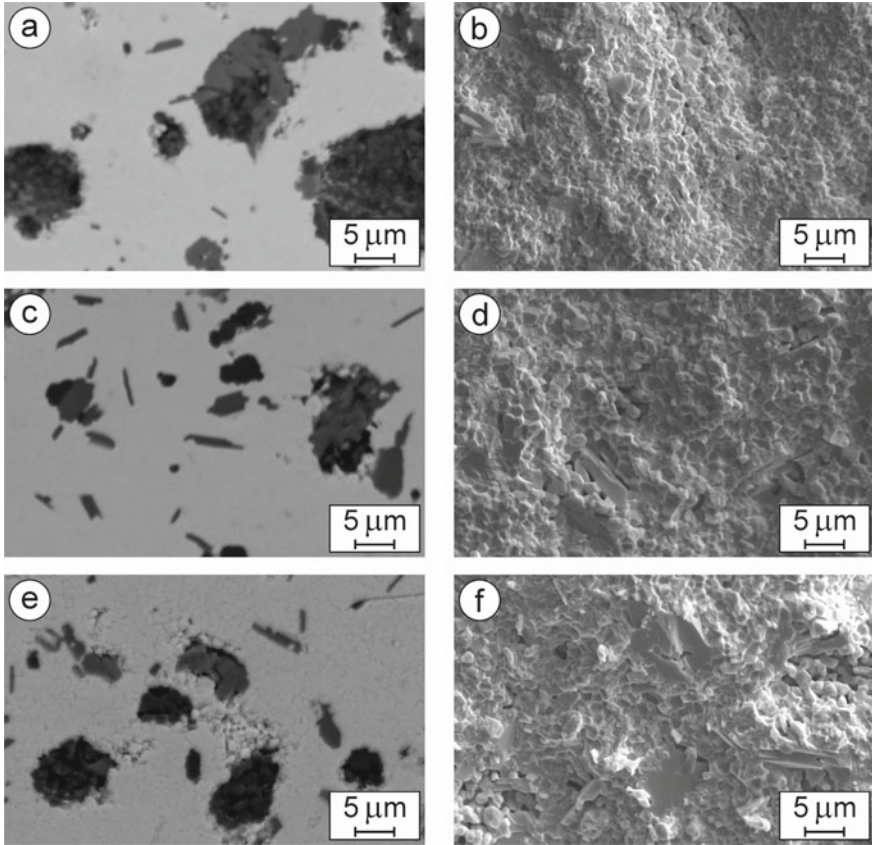


Fig. 6 SEM **a, c, e** microstructures (BSD images at high magnifications) and **b, d, f** fractography (SE images at high magnifications) of specimen series **a, b** PSZ-1550, **c, d** PSZ-1580, and **e, f** PSZ-1620 (Table 1)

4 Conclusion

In this work, a stabilizing effect of small percentages of oxides Y_2O_3 , CoO , CeO_2 , and Fe_2O_3 on zirconia ceramics has been studied.

1. It was shown that the metal oxide additives made it possible to reach the stabilization of the tetragonal ZrO_2 phase and manufacture ceramics with fine-grained microstructure.
2. The maximum transformation toughening effect in ZrO_2 - Y_2O_3 - CoO - CeO_2 - Fe_2O_3 ceramics was found to correlate with features of fracture surface morphology. Compared to the ceramic sintered at 1550 °C, slightly increased grains of the tetragonal ZrO_2 phase were revealed in the ceramic sintered at 1580 °C. The formed microstructure allowed implementing high-energy

consuming fracture micromechanism involving tetragonal to monoclinic ZrO_2 phase transformation toughening without transgranular cleavage fracture of monoclinic ZrO_2 phase particles.

Acknowledgements The authors are thankful to the staff of the Scientific Equipment Collective Use Center “Laboratory of Advanced Technologies, Creation and Physicochemical Analysis of a New Substances and Functional Materials” at Lviv Polytechnic National University (<https://lpnu.ua/cckno>) for their kind help in performing X-ray diffraction studies.

References

1. J. Chevalier, S. Deville, E. Munch et al., Critical effect of cubic phase on aging in 3 mol% yttria-stabilized zirconia ceramics for hip replacement prosthesis. *Biomaterials* **25**, 5539–5545 (2004). <https://doi.org/10.1016/j.biomaterials.2004.01.002>
2. S. Deville, L. Gremillard, J. Chevalier et al., A critical comparison of methods for the determination of the aging sensitivity in biomedical grade yttria-stabilized zirconia. *J. Biomed. Mater. Res. B Appl. Biomater.* **72B**, 239–245 (2005). <https://doi.org/10.1002/jbm.b.30123>
3. Y. Kharchenko, Z. Blikharsky, V. Vira et al., Nanostructural changes in a Ni/NiO cermet during high-temperature reduction and reoxidation, in *Nanomaterials and Nanocomposites, Nanostructure Surfaces, and Their Applications. Springer Proceedings in Physics*, vol. **246** (2021), pp. 219–229. https://doi.org/10.1007/978-3-030-51905-6_17
4. A.R. Studart, F. Filser, P. Kocher et al., Fatigue of zirconia under cycling loading in water and its implications for the design of dental bridges. *Dent. Mater.* **23**, 106–114 (2007). <https://doi.org/10.1016/j.dental.2005.12.008>
5. M. Alfano, G.D. Girolamo, L. Pagnotta et al., Processing, microstructure and mechanical properties of air plasma-sprayed ceria–yttria co-stabilized zirconia coatings. *Strain* **46**, 409–418 (2010). <https://doi.org/10.1111/j.1475-1305.2009.00659.x>
6. G.D. Girolamo, C. Blasi, M. Schioppa et al., Structure and thermal properties of heat treated plasma sprayed ceria–yttria co-stabilized zirconia coatings. *Ceram. Int.* **36**, 961–968 (2010). <https://doi.org/10.1016/j.ceramint.2009.10.020>
7. B.D. Vasylyv, V.Y. Podhurs'ka, O.P. Ostash et al., Influence of reducing and oxidizing media on the physicomechanical properties of ScCeSZ–NiO and YSZ–NiO ceramics. *Mater. Sci.* **49**(2), 135–144 (2013). <https://doi.org/10.1007/s11003-013-9593-3>
8. G. Chen, Q. Li, Y. Ling, H. Zheng, J. Chen, Q. Jiang, K. Li, J. Peng, M. Omran, L. Gao, Phase stability and microstructure morphology of microwave-sintered magnesia–partially stabilised zirconia. *Ceram. Int.* **47**, 4076–4082 (2021). <https://doi.org/10.1016/j.ceramint.2020.09.281>
9. G. Chen, Y. Ling, Q. Li et al., Crystal structure and thermomechanical properties of CaO-PSZ ceramics synthesised from fused ZrO_2 . *Ceram. Int.* **46**, 15357–15363 (2020). <https://doi.org/10.1016/j.ceramint.2020.03.079>
10. J. Chevalier, L. Gremillard, A.V. Virkar et al., The tetragonal-monoclinic transformation in zirconia: lessons learned and future trends. *J. Am. Ceram. Soc.* **92**, 1901–1920 (2009). <https://doi.org/10.1111/j.1551-2916.2009.03278.x>
11. A. Kumar, P. Kumar, A.S. Dhaliwal, Structural studies of zirconia and yttria doped zirconia for analysing its phase stabilization criteria. *IOP Conf. Ser.: Mater. Sci. Eng.* **1033**, 012052 (2021). <https://doi.org/10.1088/1757-899X/1033/1/012052>
12. A.D. Ivasyshyn, B.D. Vasylyv, Effect of the size and form of specimens on the diagram of growth rates of fatigue cracks. *Mater. Sci.* **37**(6), 1002–1004 (2001). <https://doi.org/10.1023/A:1015669913601>

13. T.K. Gupta, J.H. Bechtold, R.C. Kuznicki et al., Stabilization of tetragonal phase in polycrystalline zirconia. *J. Mater. Sci.* **12**, 2421–2426 (1977). <https://doi.org/10.1007/bf00553928>
14. H.G. Scott, Phase relationships in the zirconia–yttria system. *J. Mater. Sci.* **10**, 1527–1535 (1975). <https://doi.org/10.1007/BF01031853>
15. C. Piconi, S. Sprio, Zirconia implants: is there a future? *Curr. Oral Health Rep.* **5**, 186–193 (2018). <https://doi.org/10.1007/s40496-018-0187-x>
16. Y. Kharchenko, Z. Blikharsky, V. Vira et al., Study of nanostructural changes in a Ni-containing cermet material during reduction and oxidation at 600 °C. *Appl. Nanosci.* **10**, 4535–4543 (2020). <https://doi.org/10.1007/s13204-020-01391-1>
17. M.F.R.P. Alves, S. Ribeiro, P.A. Suzuki et al., Effect of Fe₂O₃ addition and sintering temperature on mechanical properties and translucence of zirconia dental ceramics with different Y₂O₃ content. *Mater. Res.* **24**(2), e20200402 (2021). <https://doi.org/10.1590/1980-5373-MR-2020-0402>
18. V. Podhurska, B. Vasylyv, O. Ostash et al., Influence of treatment temperature on microstructure and properties of YSZ–NiO anode materials. *Nanoscale Res. Lett.* **11**, 93 (2016). <https://doi.org/10.1186/s11671-016-1306-z>
19. H.A. Shabri, M.H.D. Othman, M.A. Mohamed et al., Recent progress in metal-ceramic anode of solid oxide fuel cell for direct hydrocarbon fuel utilization: a review. *Fuel Process. Technol.* **212**, 106626 (2021). <https://doi.org/10.1016/j.fuproc.2020.106626>
20. B. Vasylyv, V. Podhurska, O. Ostash, Preconditioning of the YSZ–NiO fuel cell anode in hydrogenous atmospheres containing water vapor. *Nanoscale Res. Lett.* **12**, 265 (2017). <https://doi.org/10.1186/s11671-017-2038-4>
21. P. Khajavi, P.V. Hendriksen, J. Chevalier et al., Improving the fracture toughness of stabilized zirconia-based solid oxide cells fuel electrode supports: effects of type and concentration of stabilizer(s). *J. Eur. Ceram. Soc.* **40**, 5670–5682 (2020). <https://doi.org/10.1016/j.jeurceram soc.2020.05.042>
22. T.A. Prikhna, O.P. Ostash, A.S. Kuprin et al., A new MAX phases-based electroconductive coating for high-temperature oxidizing environment. *Compos. Struct.* **277**, 114649 (2021). <https://doi.org/10.1016/j.compstruct.2021.114649>
23. S. Jiang, X. Huang, Z. He et al., Phase transformation and lattice parameter changes of non-trivalent rare earth-doped YSZ as a function of temperature. *J. Mater. Eng. Perform.* **27**, 2263–2270 (2018). <https://doi.org/10.1007/s11665-018-3159-3>
24. M.Y. Smyrnova-Zamkova, V.P. Red'ko, O.K. Ruban et al., The properties of nanocrystalline powder of 90% Al₂O₃–10% ZrO₂ (wt.%) obtained via the hydrothermal synthesis/mechanical mixing. *Nanosistemi. Nanomater. Nanotehnol.* **15**(2), 309–317 (2017). <https://doi.org/10.15407/nnn.15.02.0309>
25. S.S. Savka, D.I. Popovych, A.S. Serednytski, Molecular dynamics simulations of the formation processes of zinc oxide nanoclusters in oxygen environment, in *Nanophysics, Nanomaterials, Interface Studies, and Applications. Springer Proceedings in Physics*, vol 195 (2017), pp. 145–156. https://doi.org/10.1007/978-3-319-56422-7_11
26. T.A. Schaedler, R.M. Leckie, S. Kramer et al., Toughening of nontransformable t'-YSZ by addition of titania. *J. Am. Ceram. Soc.* **90**, 3896–3901 (2007). <https://doi.org/10.1111/j.1551-2916.2007.01990.x>
27. M. Zhao, W. Pan, C. Wan et al., Defect engineering in development of low thermal conductivity materials: a review. *J. Eur. Ceram. Soc.* **37**, 1–13 (2016). <https://doi.org/10.1016/j.jeurceram soc.2016.07.036>
28. A.J. Santos, S. Garcia-Segura, S. Dosta et al., A ceramic electrode of ZrO₂–Y₂O₃ for the generation of oxidant species in anodic oxidation. Assessment of the treatment of Acid Blue 29 dye in sulfate and chloride media. *Sep. Purif. Technol.* **228**, 115747 (2019). <https://doi.org/10.1016/j.seppur.2019.115747>
29. Y. Yan, Z. Ma, J. Sun et al., Surface microstructure-controlled ZrO₂ for highly sensitive room-temperature NO₂ sensors. *Nano. Mater. Sci.* **3**, 268–275 (2021). <https://doi.org/10.1016/j.nanos.2021.02.001>

30. B. Vasylyv, J. Milewski, V. Podhurska et al., Study of the degradation of a fine-grained YSZ–NiO anode material during reduction in hydrogen and reoxidation in air. *Appl. Nanosci.* **12**, 965–975 (2022). <https://doi.org/10.1007/s13204-021-01768-w>
31. A.D. Bona, O.E. Pecho, R. Alessandretti, Zirconia as a dental biomaterial. *Materials* **8**, 4978–4991 (2015). <https://doi.org/10.3390/ma8084978>
32. J. Gui, Z. Xie, Phase transformation and slow crack growth study of Y-TZP dental ceramic. *Mater. Sci. Eng. A* **676**, 531–535 (2016). <https://doi.org/10.1016/j.msea.2016.09.026>
33. D. Li, Y. Liu, Y. Zhong et al., Dense and strong ZrO₂ ceramics fully densified in <15 min. *Adv. Appl. Ceram.* **118**, 23–29 (2019). <https://doi.org/10.1080/17436753.2018.1449580>
34. N. Juntavee, S. Attashu, Effect of different sintering process on flexural strength of translucency monolithic zirconia. *J. Clin. Exp. Dent.* **10**, e821–e830 (2018). <https://doi.org/10.4317/jced.54749>
35. J. Zou, Y. Zhong, M. Eriksson et al., Tougher zirconia nanoceramics with less yttria. *Adv. Appl. Ceram.* **118**, 9–15 (2018). <https://doi.org/10.1080/17436753.2018.1445464>
36. R. Chintapalli, A. Mestra, F.G. Marro et al., Stability of nanocrystalline spark plasma sintered 3Y-TZP. *Materials* **3**, 800–814 (2010). <https://doi.org/10.3390/ma3020800>
37. B. Stawarczyk, M. Özcan, L. Hallmann et al., The effect of zirconia sintering temperature on flexural strength, grain size, and contrast ratio. *Clin. Oral Invest.* **17**, 269–274 (2013). <https://doi.org/10.1007/s00784-012-0692-6>
38. M. Amaral, P.F. Cesar, M.A. Bottino et al., Fatigue behavior of Y-TZP ceramic after surface treatments. *J. Mech. Behav. Biomed. Mater.* **57**, 149–156 (2016). <https://doi.org/10.1016/j.jmbbm.2015.11.042>
39. M.J. Kim, J.S. Ahn, J.H. Kim et al., Effects of the sintering conditions of dental zirconia ceramics on the grain size and translucency. *J. Adv. Prosthodont.* **5**, 161–166 (2013). <https://doi.org/10.4047/jap.2013.5.2.161>
40. M. Guazzato, M. Albakry, S.P. Ringer et al., Strength, fracture toughness and microstructure of a selection of all-ceramic materials. Part II Zirconia-based dental ceramics. *Dent. Mater.* **20**, 449–456 (2004). <https://doi.org/10.1016/j.dental.2003.05.003>
41. C. Gautam, J. Joyner, A. Gautam et al., Zirconia based dental ceramics: structure, mechanical properties, biocompatibility and applications. *Dalton Trans.* **45**, 19194–19215 (2016). <https://doi.org/10.1039/c6dt03484e>
42. J. Chevalier, What future for zirconia as a biomaterial? *Biomaterials* **27**, 535–543 (2006). <https://doi.org/10.1016/j.biomaterials.2005.07.034>
43. C.G. Soubelet, M.P. Albano, Differences in microstructure and mechanical properties between Y-TZP and Al₂O₃-doped Y-TZP/bioglass ceramics. *Int. J. Appl. Ceram. Technol.* **18**, 2237–2249 (2021). <https://doi.org/10.1111/ijac.13864>
44. M. Trunec, K. Castkova, P. Roupčova, Effect of phase structure on sintering behavior of zirconia nanopowders. *J. Am. Ceram. Soc.* **96**, 3720–3727 (2013). <https://doi.org/10.1111/jace.12624>
45. P. Duràn, M. Villegas, J.F. Fernández et al., Theoretically dense and nanostructured ceramics by pressureless sintering of nanosized Y-TZP powders. *Mater. Sci. Eng* **A232**, 168–176 (1997). [https://doi.org/10.1016/S0921-5093\(97\)00099-3](https://doi.org/10.1016/S0921-5093(97)00099-3)
46. L. Li, O. Van Der Biest, P.L. Wang et al., Estimation of the phase diagram for the ZrO₂–Y₂O₃–CeO₂ system. *J. Eur. Ceram. Soc.* **21**(16), 2903–2910 (2001). [https://doi.org/10.1016/S0955-2219\(01\)00218-7](https://doi.org/10.1016/S0955-2219(01)00218-7)
47. J.A. Allemann, B. Michel, H.B. Märki et al., Grain growth of differently doped zirconia. *J. Eur. Ceram. Soc.* **15**(10), 951–958 (1995). [https://doi.org/10.1016/0955-2219\(95\)00073-4](https://doi.org/10.1016/0955-2219(95)00073-4)
48. N.M. Ersoy, H.M. Aydoğdu, B.U. Değirmenci et al., The effects of sintering temperature and duration on the flexural strength and grain size of zirconia. *Acta Biomater. Odontol. Scand.* **1**(2–4), 43–50 (2015). <https://doi.org/10.3109/23337931.2015.1068126>
49. T. Sakuma, Y. Yoshizawa, The grain growth of zirconia during annealing in the cubic/tetragonal two-phase region. *Mater. Sci. Forum* **94–96**, 865–870 (1992). <https://doi.org/10.4028/www.scientific.net/MSF.94-96.865>

50. B. Stawarczyk, A. Emslander, M. Roos et al., Zirconia ceramics, their contrast ratio and grain size depending on sintering parameters. *Dent. Mater. J.* **33**(5), 591–598 (2014). <https://doi.org/10.4012/dmj.2014-056>
51. M. Vojtko, V. Puchy, E. Múdra et al., Coarse-grain CeO₂ doped ZrO₂ ceramic prepared by spark plasma sintering. *J. Eur. Ceram. Soc.* **40**, 4844–4852 (2020). <https://doi.org/10.1016/j.jeurceramsoc.2020.05.014>
52. J. Grabis, D. Jankoviča, I. Šteins et al., Characteristics and sinterability of ceria stabilized zirconia nanoparticles prepared by chemical methods. *Mater. Sci.* **24**(3), 243–246 (2018). <https://doi.org/10.5755/j01.ms.24.3.18288>
53. A. Gupta, S. Sharma, N. Mahato et al., Mechanical properties of spark plasma sintered ceria reinforced 8 mol% yttria-stabilized zirconia electrolyte. *Nanomater. Energy* **1**(NME5), 306–315 (2012). <https://doi.org/10.1680/nme.12.00018>
54. M. Ahsanzadeh-Vadeqani, R.S. Razavi, Spark plasma sintering of zirconia-doped yttria ceramic and evaluation of the microstructure and optical properties. *Ceram. Int.* **42**(16), 18931–18936 (2016). <https://doi.org/10.1016/j.ceramint.2016.09.043>
55. L. An, A. Ito, T. Goto, Transparent yttria produced by spark plasma sintering at moderate temperature and pressure profiles. *J. Eur. Ceram. Soc.* **32**(5), 1035–1040 (2012). <https://doi.org/10.1016/j.jeurceramsoc.2011.11.023>
56. S. Kikuchi, K. Katahira, J. Komotori, Formation of titanium/zirconia based biomaterial fabricated by spark plasma sintering. *J. Japan Inst. Met. Mater.* **82**(9), 341–348 (2018). <https://doi.org/10.2320/jinstmet.J2018017>
57. Á.G. López, C.L. Pernía, C.M. Ferreira et al., Spark plasma sintered zirconia ceramic composites with graphene-based nanostructures. *Ceramics* **1**(1), 153–164 (2018). <https://doi.org/10.3390/ceramics1010014>
58. E.F. Garcia, C.F.G. Gonzalez, A. Fernandez et al., Processing and spark plasma sintering of zirconia/titanium cermets. *Ceram. Int.* **39**(6), 6931–6936 (2013). <https://doi.org/10.1016/j.ceramint.2013.02.029>
59. Y.G. Chabak, V.I. Fedun, K. Shimizu et al., Phase-structural composition of coating obtained by pulsed plasma treatment using eroded cathode of T1 high speed steel. *Probl. At Sci. Technol.* **104**(4), 100–106 (2016)
60. O.M. Romaniv, I.V. Zalite, V.M. Simin'kovych et al., Effect of the concentration of zirconium dioxide on the fracture resistance of Al₂O₃–ZrO₂ ceramics. *Mater. Sci.* **31**(5), 588–594 (1996). <https://doi.org/10.1007/BF00558793>
61. O.M. Romaniv, B.D. Vasylyv, Some features of formation of the structural strength of ceramic materials. *Mater. Sci.* **34**(2), 149–161 (1998). <https://doi.org/10.1007/BF02355530>
62. V.V. Kulyk, Z.A. Duriagina, B.D. Vasylyv et al., Effects of yttria content and sintering temperature on the microstructure and tendency to brittle fracture of yttria-stabilized zirconia. *Arch. Mater. Sci. Eng.* **109**(2), 65–79 (2021). <https://doi.org/10.5604/01.3001.0015.2625>
63. V. Kulyk, Z. Duriagina, B. Vasylyv et al., The effect of sintering temperature on the phase composition, microstructure, and mechanical properties of yttria-stabilized zirconia. *Materials* **15**, 2707 (2022). <https://doi.org/10.3390/ma15082707>
64. Y. Zhang, K. Shimizu, X. Yaer et al., Erosive wear performance of heat treated multi-component cast iron containing Cr, V, Mn and Ni eroded by alumina spheres at elevated temperatures. *Wear* **390–391**, 135–145 (2017). <https://doi.org/10.1016/j.wear.2017.07.017>
65. Q.L. Li, Y.Y. Jiang, Y.R. Wei et al., The influence of yttria content on the microstructure, phase stability and mechanical properties of dental zirconia. *Ceram. Int.* **48**, 5361–5368 (2022). <https://doi.org/10.1016/j.ceramint.2021.11.079>
66. V. Kulyk, Z. Duriagina, A. Kostryzhev et al., The effect of yttria content on microstructure, strength, and fracture behavior of yttria-stabilized zirconia. *Materials* **15**, 5212 (2022). <https://doi.org/10.3390/ma15155212>
67. ASTM E 384-11, Standard test method for Knoop and Vickers hardness of materials (ASTM International, 2011). <https://doi.org/10.1520/E0384-11>
68. ASTM C 1327-03, Standard test method for Vickers indentation hardness of advanced ceramics (ASTM International, 2003). <https://doi.org/10.1520/C1327-03>

69. V.I. Zurnadzhy, V.G. Efremenko, I. Petryshynets et al., Mechanical properties of carbide-free lower bainite in complex-alloyed constructional steel: effect of bainitizing treatment parameters. *Kov Mater.* **58**(2), 129–140 (2020). https://doi.org/10.4149/km_2020_2_129
70. B.R. Lawn, M.V. Swain, Microfracture beneath point indentations in brittle solids. *J. Mater. Sci.* **10**(1), 113–122 (1975). <https://doi.org/10.1007/BF00541038>
71. B.R. Lawn, E.R. Fuller, Equilibrium penny-like cracks in indentation fracture. *J. Mater. Sci.* **10**(12), 2016–2024 (1975). <https://doi.org/10.1007/BF00557479>
72. A.G. Evans, E.A. Charles, Fracture toughness determinations by indentation. *J. Am. Ceram. Soc.* **59**(7–8), 371–372 (1976). <https://doi.org/10.1111/j.1151-2916.1976.tb10991.x>
73. R.F. Cook, G.M. Pharr, Direct observation and analysis of indentation cracking in glasses and ceramics. *J. Am. Ceram. Soc.* **73**(4), 787–817 (1990). <https://doi.org/10.1111/j.1151-2916.1990.tb05119.x>
74. B.R. Lawn, in *Fracture of Brittle Solids*, 2nd edn (Cambridge, 1993). <https://doi.org/10.1017/CBO9780511623127>
75. K. Tanaka, Elastic/plastic indentation hardness and indentation fracture toughness: the inclusion core model. *J. Mater. Sci.* **22**(4), 1501–1508 (1987). <https://doi.org/10.1007/BF01233154>
76. K. Niihara, R. Morena, D.P.H. Hasselman, Evaluation of K_{Ic} of brittle solids by the indentation method with low crack-to-indent ratios. *J. Mater. Sci. Lett.* **1**(1), 13–16 (1982). <https://doi.org/10.1007/BF00724706>
77. K. Niihara, A fracture mechanics analysis of indentation-induced Palmqvist crack in ceramics. *J. Mater. Sci. Lett.* **2**(5), 221–223 (1983). <https://doi.org/10.1007/BF00725625>
78. J.E. Blendell, The origins of internal stresses in polycrystalline alumina and their effects on mechanical properties (Cambridge, 1979). <http://hdl.handle.net/1721.1/44234>
79. B.R. Lawn, A.G. Evans, D.B. Marshall, Elastic/plastic indentation damage in ceramics: the median/radial crack system. *J. Am. Ceram. Soc.* **63**(9–10), 574–581 (1980). <https://doi.org/10.1111/j.1151-2916.1980.tb10768.x>
80. A. Nastic, A. Merati, M. Bielawski et al., Instrumented and Vickers indentation for the characterization of stiffness, hardness and toughness of zirconia toughened Al_2O_3 and SiC armor. *J. Mater. Sci. Technol.* **31**(8), 773–783 (2015). <https://doi.org/10.1016/j.jmst.2015.06.005>
81. G.R. Anstis, P. Chantikul, B.R. Lawn et al., A critical evaluation of indentation techniques for measuring fracture toughness: I, Direct crack measurement. *J. Am. Ceram. Soc.* **64**(9), 533–538 (1981). <https://doi.org/10.1111/j.1151-2916.1981.tb10320.x>
82. M.Y. Smyrnova-Zamkova, O.K. Ruban, O.I. Bykov et al., The influence of the ZrO_2 solid solution amount on the physicochemical properties of Al_2O_3 – ZrO_2 – Y_2O_3 – CeO_2 powders. *Powder Metall. Met. Ceram.* **60**(3–4), 129–141 (2021). <https://doi.org/10.1007/s11106-021-00222-4>
83. J. Lankford, Indentation microfracture in the Palmqvist crack regime: implications for fracture toughness evaluation by the indentation method. *J. Mater. Sci. Lett.* **1**(11), 493–495 (1982). <https://doi.org/10.1007/BF00721938>
84. B. Vasylyv, V. Kulyk, Z. Duriagina et al., Estimation of the effect of redox treatment on microstructure and tendency to brittle fracture of anode materials of YSZ–NiO(Ni) system. *East Eur. J. Enterp. Technol.* **108/6**(12), 67–77 (2020). <https://doi.org/10.15587/1729-4061.2020.218291>
85. B.D. Vasylyv, V.Y. Podhurska, O.P. Ostash et al., Effect of a hydrogen sulfide-containing atmosphere on the physical and mechanical properties of solid oxide fuel cell materials, in *Nanochemistry, Biotechnology, Nanomaterials, and Their Applications. Springer Proceedings in Physics*, vol. 214 (2018), pp. 475–485. https://doi.org/10.1007/978-3-319-92567-7_30
86. J.M. Gere, S.P. Timoshenko, *Mechanics of Materials*, 4th edn. (PWS Publishing Company, Boston, MA, USA, 1997), p.912
87. ASTM E 399-20a, Standard test method for linear-elastic plane-strain fracture toughness of metallic materials (ASTM International, 2020). <https://doi.org/10.1520/E0399-20A>
88. ASTM C 1421-18, Standard test methods for determination of fracture toughness of advanced ceramics at ambient temperature (ASTM International, 2018). <https://doi.org/10.1520/C1421-18>

89. J. Kübier, Fracture toughness of ceramics using the SEVNB method: from a preliminary study to a standard test method, ed. by J. Salem et al., in *Fracture Resistance Testing of Monolithic and Composite Brittle Materials* (ASTM International, 2002), pp. 93–106. <https://doi.org/10.1520/STP10473S>
90. M. Ettler, G. Blaß, N.H. Menzler, Characterization of Ni–YSZ-cermets with respect to redox stability. *Fuel Cells* **7**(5), 349–355 (2007). <https://doi.org/10.1002/fuce.200700007>
91. B.D. Vasylyv, Initiation of a crack from the edge of a notch with oblique front in specimens of brittle materials. *Mater. Sci.* **38**(5), 724–728 (2002). <https://doi.org/10.1023/A:1024222709514>
92. M. Radovic, E. Lara-Curzio, Mechanical properties of tape cast nickel-based anode materials for solid oxide fuel cells before and after reduction in hydrogen. *Acta Mater.* **52**(20), 5747–5756 (2004). <https://doi.org/10.1016/j.actamat.2004.08.023>
93. V.V. Kulyk, B.D. Vasylyv, Z.A. Duriagina et al., The effect of water vapor containing hydrogenous atmospheres on the microstructure and tendency to brittle fracture of anode materials of YSZ–NiO(Ni) system. *Arch. Mater. Sci. Eng.* **108**(2), 49–67 (2021). <https://doi.org/10.5604/01.3001.0015.0254>
94. T.B. Serbenyuk, T.O. Prikhna, V.B. Sverdun et al., Effect of the additive of Y₂O₃ on the structure formation and properties of composite materials based on AlN–SiC. *J. Superhard. Mater.* **40**(1), 8–15 (2018). <https://doi.org/10.3103/S1063457618010021>
95. M.Y. Smyrnova-Zamkova, O.K. Ruban, O.I. Bykov, et al., Physico-chemical properties of fine-grained powder in Al₂O₃–ZrO₂–Y₂O₃–CeO₂ system produced by combined method. *Comp. Theory Pract.* **18**(4), 234–240 (2018). https://kompozyty.ptmk.net/pliczki/pliki/1290_2018t04_maria-y-smyrnova-zamkova-.pdf
96. M. Andrzejczuk, O. Vasylyev, I. Brodnikovskiy et al., Microstructural changes in NiO–ScSZ composite following reduction processes in pure and diluted hydrogen. *Mater. Charact.* **87**, 159–165 (2014). <https://doi.org/10.1016/j.matchar.2013.11.011>
97. Y. Wang, M.E. Walter, K. Sabolsky et al., Effects of powder sizes and reduction parameters on the strength of Ni–YSZ anodes. *Solid State Ionics* **177**, 1517–1527 (2006). <https://doi.org/10.1016/j.ssi.2006.07.010>
98. J.W. Adams, R. Ruh, K.S. Mazdiyasi, Young’s modulus, flexural strength, and fracture of yttria-stabilized zirconia versus temperature. *J. Am. Ceram. Soc.* **80**(4), 903–908 (1997). <https://doi.org/10.1111/j.1151-2916.1997.tb02920.x>
99. O.P. Ostash, B.D. Vasylyv, V.Y. Podhurs’ka, et al., Optimization of the properties of 10Sc1CeSZ–NiO composite by the redox treatment. *Mater. Sci.* **46**(5):653–658 (2011). <https://doi.org/10.1007/s11003-011-9337-1>
100. B.D. Vasylyv, Improvement of the electric conductivity of the material of anode in a fuel cell by the cyclic redox thermal treatment. *Mater. Sci.* **46**(2), 260–264 (2010). <https://doi.org/10.1007/s11003-010-9282-4>
101. I. Danilenko, G. Lasko, I. Brykhanova et al., The peculiarities of structure formation and properties of zirconia-based nanocomposites with addition of Al₂O₃ and NiO. *Nanoscale Res. Lett.* **12**, 125 (2017). <https://doi.org/10.1186/s11671-017-1901-7>
102. V.Y. Podhurs’ka, B.D. Vasylyv, O.P. Ostash et al., Structural transformations in the NiO-containing anode of ceramic fuel cells in the course of its reduction and oxidation. *Mater. Sci.* **49**(6), 805–811 (2014). <https://doi.org/10.1007/s11003-014-9677-8>
103. I. Danilenko, F. Glazunov, T. Konstantinova et al., Effect of Ni/NiO particles on structure and crack propagation in zirconia based composites. *Adv. Mater. Lett.* **5**(8), 465–471 (2014). <https://doi.org/10.5185/amlett.2014.amwc1040II>
104. G.A. Gogotsi, S.N. Dub, E.E. Lomonova et al., Vickers and Knoop indentation behaviour of cubic and partially stabilized zirconia crystals. *J. Eur. Ceram. Soc.* **15**(5), 405–413 (1995). [https://doi.org/10.1016/0955-2219\(95\)91431-M](https://doi.org/10.1016/0955-2219(95)91431-M)
105. B.D. Vasylyv, A procedure for the investigation of mechanical and physical properties of ceramics under the conditions of biaxial bending of a disk specimen according to the ring–ring scheme. *Mater. Sci.* **45**(4), 571–575 (2009). <https://doi.org/10.1007/s11003-010-9215-2>

106. O.N. Grigoriev, V.B. Vinokurov, T.V. Mosina et al., Kinetics of shrinkage, structurization, and the mechanical characteristics of zirconium boride sintered in the presence of activating additives. *Powder Metall. Met. Ceram.* **55**(11–12), 676–688 (2017). <https://doi.org/10.1007/s11106-017-9855-y>
107. Z. Peng, J. Gong, H. Miao, On the description of indentation size effect in hardness testing for ceramics: analysis of the nanoindentation data. *J. Eur. Ceram. Soc.* **24**, 2193–2201 (2004). [https://doi.org/10.1016/s0955-2219\(03\)00641-1](https://doi.org/10.1016/s0955-2219(03)00641-1)
108. V.V. Rodaev, A.O. Zhigachev, A.I. Tyurin et al., An engineering zirconia ceramic made of baddeleyite. *Materials* **14**, 4676 (2021). <https://doi.org/10.3390/ma14164676>